UCRL-JRNL-206134

LAWRENCE LIVERMORE NATIONAL LABORATORY

Synthesis and Electronic Structure of Low-Density Monoliths of Nanoporous Nanocrystalline Anatase TiO_2

S. O. Kucheyev, T. F. Baumann, Y. M. Wang, T. van Buuren and J. H. Satcher, Jr.

August 16, 2004

Journal of Electron Spectroscopy and Related Phenomena

This document was prepared as an account of work sponsored by an agency of the United States Government. Neither the United States Government nor the University of California nor any of their employees, makes any warranty, express or implied, or assumes any legal liability or responsibility for the accuracy, completeness, or usefulness of any information, apparatus, product, or process disclosed, or represents that its use would not infringe privately owned rights. Reference herein to any specific commercial product, process, or service by trade name, trademark, manufacturer, or otherwise, does not necessarily constitute or imply its endorsement, recommendation, or favoring by the United States Government or the University of California. The views and opinions of authors expressed herein do not necessarily state or reflect those of the United States Government or the University of California, and shall not be used for advertising or product endorsement purposes.

Updated October 14, 2003

Prepared for J. Electron Spectr. Relat. Phenom.

Synthesis and electronic structure of low-density monoliths of nanoporous nanocrystalline anatase TiO_2

S. O. Kucheyev,* T. F. Baumann, Y. M. Wang, T. van Buuren, and J. H. Satcher, Jr.
Lawrence Livermore National Laboratory, Livermore, California 94550
(Dated: August 13, 2004)

Monolithic nanocrystalline anatase titania aerogels are synthesized by the epoxide sol-gel method followed by thermal annealing at 550 °C. These aerogels are formed by ∼10–20 nm size anatase nanoparticles which are randomly oriented and interconnected into an open-cell solid network. Aerogel monoliths have an apparent density of ∼6% and a surface area of ∼ 100 m^2 g^{-1}. High-resolution transmission electron microscopy and soft x-ray absorption near-edge structure spectroscopy reveal good crystallinity of the anatase nanoparticles forming the aerogel skeleton.

PACS numbers: 71.20.Be, 78.70.Dm, 71.23.Cq, 82.70.Rr

I. INTRODUCTION

Titanium dioxide (TiO_2) is a technologically important wide band-gap transition metal oxide. It finds numerous applications in areas such as heterogeneous catalysis, solar cells, optical and corrosion coatings, gas sensors, varistors, and pigments in paints and cosmetic products (see, for example, a recent review [1]). In recent years, synthesis and properties of nanostructured TiO_2 have attracted considerable research interest. Most of such research efforts have focused on titania nanoparticles and nanopowders [1], and only a few reports on nanostructured nanoporous TiO_2 monoliths have appeared in the literature (see, for example, reviews [2, 3]). Such nanoporous titania monoliths are typically sol-gel-derived open-cell solid foams. The lowest apparent density (i.e., the highest porosity) material is obtained by drying highly cross-linked wet gels under supercritical conditions. The resultant materials are called aerogels. They typically exhibit a high degree of porosity (mesaporosity), with ultrafine, nanometer size cells/pores [2–6].

In our recent report [6], we discussed synthesis and the electronic structure of low-density (< 10% relative density) TiO_2 aerogel monoliths. Such aerogels were formed by ∼10–20 nm in size fully amorphous TiO_2 particles interconnected into a treelike skeleton of the gel. In the present article, we show that thermal annealing under certain conditions can recrystallize initially amorphous nanoligaments of titania aerogels into the anatase phase without collapse of the monolith into powder. We study the morphology and the electronic structure of nanocrystalline aerogels by high-resolution transmission electron microscopy (TEM) and soft x-ray absorption near-edge structure (XANES) spectroscopy, respectively.

*Email address: kucheyev1@llnl.gov

II. EXPERIMENTAL

The following samples were investigated in this study: titania aerogels before and after thermal annealing as well as rutile and anatase powder references (with grain sizes $\gtrsim$ 5μm). Such TiO_2 powders were purchased from Sigma-Aldrich Corp. The TiO_2 aerogels were prepared by a two-step sol-gel process that involved acid-catalyzed hydrolysis of titanium ethoxide, followed by base-initiated gelation of the titania species, as described in detail elsewhere [6]. As-synthesized aerogels were annealed at 550 °C for 1 hour in air with a temperature ramp rate of 5 degrees per minute. It is important to note that aerogels remained monolithic after such an annealing step.

The bulk densities of the aerogels were determined by measuring the dimensions and mass of monolithic samples. Surface area determination and pore volume and size analysis were performed by Brunauer-Emmett-Teller (BET) and Barrett-Joyner-Halenda (BJH) methods [7] using an ASAP 2000 Surface Area Analyzer (Micromeritics Instrument Corp.). Samples of ∼0.1 g were heated to 150 °C under vacuum (10^{-5} torr) for $\gtrsim$24 hours to remove adsorbed species. Nitrogen adsorption data were then taken at five relative pressures from 0.05 to 0.20 at −196 °C to calculate the surface area by BET theory. For BJH analysis, average pore size and pore volume were calculated using data points from the desorption branch of the isotherm. The microstructure of aerogels was studied by high-resolution TEM in a Philips CM300FEG transmission electron microscope operating at 300 kV. The TEM images were taken under bright-field (BF) conditions and slightly defocussed to increase contrast.

The XANES experiments were performed at room temperature at undulator beamline 8.0 at the Advanced Light Source (ALS), Lawrence Berkeley National Laboratory. Details of the beamline have been published elsewhere [8]. Aerogels and TiO_2 powders were pressed into an indium metal foil and mounted on the sample holder. All spectra were obtained by measuring the total electron yield (TEY) by monitoring the total sample

TABLE I: Some properties of amorphous (as-synthesized) and anatase (annealed) titania aerogels.

	Apparent Density ($mg\ cm^{-3}$)	Porosity (%)	Surface Area ($m^2\ g^{-1}$)	Pore Volume ($cm^3\ g^{-1}$)	Average Pore Diameter (nm)
Amorphous	180	96	290	0.68	12
Anatase	260	94	96	1.43	52

photocurrent. The incoming radiation flux was monitored by the total photocurrent produced in a clean Au mesh inserted into the beam. The overall experimental resolution around the Ti $L_{2,3}$ edge was $\sim$ 150 meV. The monochromator was calibrated by aligning the Ti L_3 and O K edges of rutile powders according to values from [9]. After a linear background subtraction, all spectra were normalized to the post-edge step heights.

III. RESULTS AND DISCUSSION

Table I summarizes apparent densities, porosities, and results of the nitrogen adsorption/desorption analysis for as-synthesized and annealed titania aerogels. It is seen from Table I that the as-synthesized (fully amorphous) material is highly porous with the surface area comparable to that reported previously for titania aerogels synthesized by other sol-gel methods (i.e., $\sim$50–700 $m^2\ g^{-1}$) [2–4]. Table I also shows that annealing at 550 °C results in an expected slight decrease in the porosity and surface area and an associated increase in the average pore diameter and pore volume. However, annealed aerogels still exhibit desirable relatively high surface area and ultra-low density.

The morphology of annealed aerogels is illustrated in BF TEM images in Fig. 1. The low-magnification image in Fig. 1(a) shows that, similar to the case of as-synthesized titania aerogels studied in [6], the aerogel skeleton is formed by $\sim$10–20 nm irregular particles interconnected into a treelike structure. Some preferential faceting of the nanoparticles can also be seen in Fig. 1(a). The inset in Fig. 1(a) shows a selected-area diffraction pattern (SAD) taken from multiple nanoparticles forming the aerogel skeleton. This SAD pattern is indexed to the anatase phase of TiO_2, and no contribution from either rutile or brookite phase has been identified. In addition, the continuous SAD ring pattern suggests that the anatase nanocrystals forming the aerogel solid network are randomly oriented. Such a recrystallization into the anatase phase for the annealing conditions of this study (i.e., 550 °C) is consistent with numerous previous studies of thermal annealing behavior of amorphous TiO_2 nanoparticles (see, for example, [10]). It should also be noted that anatase is generally believed to have a superior activity in catalytic, photovoltaic, and gas sensor applications than the other common polymorphs of TiO_2 (i.e., amorphous, rutile, and brookite) [1]. Hence, the development of the anatase titania aerogel system could have important technological implications.

The structure of a typical individual nanoligament of annealed aerogels is better illustrated in a high-resolution image in Fig. 1(b). Interestingly, Fig. 1(b) reveals that, during thermal processing, individual elongated fully amorphous nanoligaments in as-synthesized aerogels (studied in [6]) recrystallize not as elongated nanocrystals but as several interconnected and randomly oriented anatase nanocrystals [$\sim$10 nm in size for the particular case shown in Fig. 1(b)] with the aspect ratio close to unity. One of such nanocrystalline particles is marked by a dotted box in Fig. 1(b).

Figure 2 gives a comparison of O K-edge [Fig. 2(a)] and Ti $L_{2,3}$-edge [Fig. 2(b)] XANES spectra of as-synthesized (amorphous) and annealed aerogels as well as rutile and anatase powder references. Spectra of rutile and anatase powders, shown in Fig. 2, are in general agreement with results of a number of previous studies and, together with the spectral features of amorphous titania aerogels, have been discussed in detail in our recent report [6]. In brief, the O K-edge XANES spectra of rutile and anatase can be well explained with single-electron approximation models [11]. Hence, these spectra essentially map the O $2p$-projected density of empty states in TiO_2. In the molecular orbital picture of TiO_2 [9, 11, 12], the conduction band, which is probed in XANES experiments, is formed by antibonding Ti $3d$, $4s$, and $4p$ and O $2p$ orbitals. In addition, the crystal field of the surrounding O atoms splits the Ti $3d$ band into t_{2g} (formed by d_{xy}, d_{xz}, and d_{yz} orbitals) and e_g (formed by $d_{x^2-y^2}$ and d_{z^2} orbitals) sub-bands. Hence, the two main peaks at $\sim$ 531 and 534 eV in Fig. 2(a) can be attributed to the excitation from the O $1s$ core level into the t_{2g} and e_g bands, respectively, and peaks at higher energies are due to transitions into antibonding O $2p$ and Ti $4sp$-related bands [9, 11, 12].

In contrast to the O K-edge spectra, Ti $L_{2,3}$-edge spectra, reflecting transitions of Ti $2p$ core electrons into Ti $3d$ states in the conduction band, show a considerably more complex behavior due to electron correlation effects. In Fig. 2(b), peaks are split into two groups, separated by $\sim$ 5.5 eV, due to the spin-orbit coupling of Ti $2p$ core electrons, giving rise to L_2 and L_3 edges. For both L_2 and L_3 edges, the crystal field splits the $3d$ band into t_{2g} and e_g sub-bands, as discussed above for O K-edge spectra.

Figure 2 shows that annealed aerogels exhibit the same spectral features as anatase powder standards (not as the rutile or amorphous phase of TiO_2). This supports

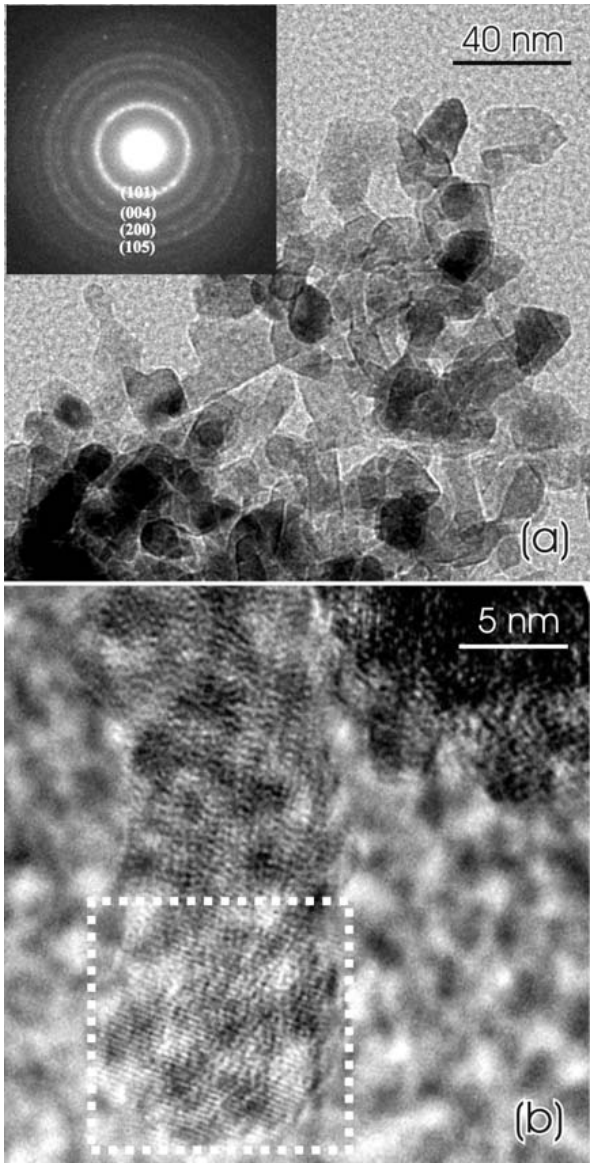

FIG. 1: High-resolution TEM images of an annealed titania aerogel at different magnifications. The inset in (a) shows a selected-area diffraction pattern taken from multiple nanoparticles forming the aerogel. The pattern is indexed to the anatase phase of TiO_2. The dotted box in (b) denotes an individual single-crystalline anatase nanoparticle.

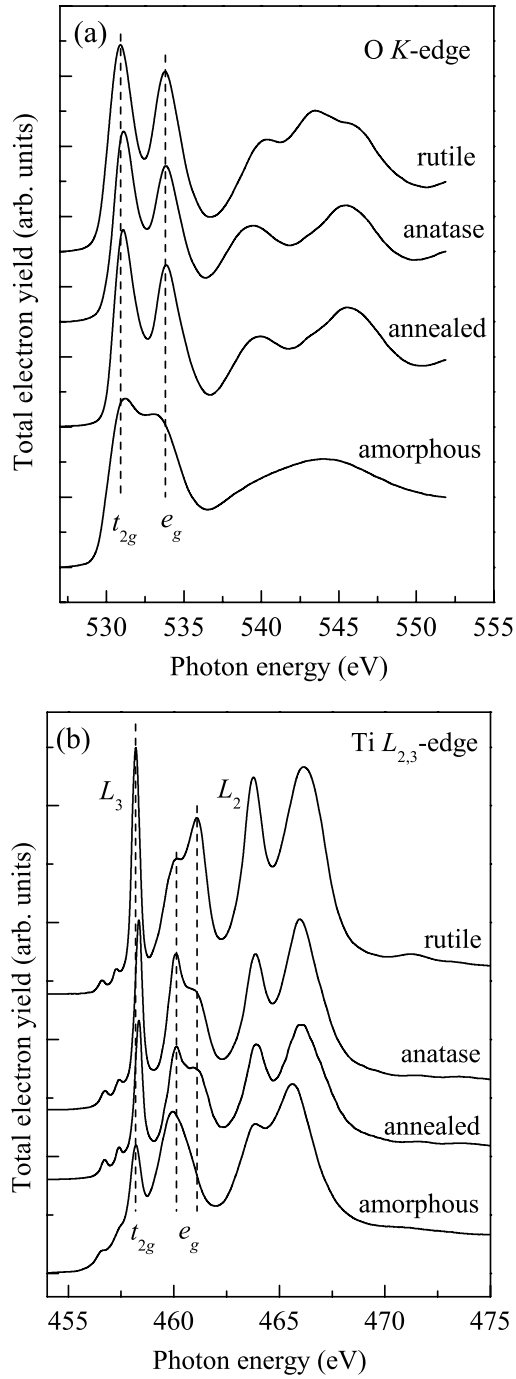

FIG. 2: Oxygen K-edge (a) and Ti $L_{2,3}$-edge (b) XANES spectra of as-synthesized (amorphous) and annealed aerogels as well as rutile and anatase powder references.

the above TEM results that annealed aerogels consist of anatase TiO_2 nanocrystals. However, Fig. 2 also shows that normalized peak intensities are slightly different for anatase micro-powders and annealed nanocrystalline anatase aerogels. A detailed investigation of such an effect of the surface atom fraction in TiO_2 aerogels on the their electronic properties is a subject of our future studies. It should be noted that previous few XANES studies of this effect in TiO_2 nanoparticles have been somewhat inconclusive and resulted in controversial interpretations [13–15]. This situation is not unexpected since a number of factors, which are difficult to control, can affect XANES spectra of TiO_2 nanoparticles, including surface reconstruction and passivation, stress, the contribution from an amorphous phase (since the amorphous phase of TiO_2 is stable at ambient conditions in contrast to the case of many other more ionic binary compounds), particle–particle and particle–support interaction, quan-

tum confinement, and charging. Hence, the effects of the particle size and surface atom fraction on the electronic density of states in the anatase TiO_2 system currently warrant additional systematic studies.

IV. CONCLUSIONS

In conclusion, we have reported on the successful synthesis of monolithic nanocrystalline anatase titania aerogels with a porosity of ∼94%. Results have shown that these aerogels are formed by ∼10–20 nm size anatase nanoparticles randomly oriented and interconnected into an open-cell solid network.

V. ACKNOWLEDGMENTS

This work was performed under the auspices of the U.S. DOE by the University of California, LLNL under Contract No. W-7405-Eng-48. The ALS is supported by the Director, Office of Science, Office of BES, Materials Sciences Division, of the U.S. DOE under Contract No. DE-AC03-76SF00098 at LBNL.

[1] U. Diebold, Surf. Sci. Rep. **48**, 53 (2003).
[2] N. Hüsing and U. Schubert, Angew. Chem. Int. Ed. **37**, 22 (1998).
[3] T. F. Baumann, A. E. Gash, G. A. Fox, J. H. Satcher, Jr., and L. W. Hrubesh, in *Handbook of Porous Solids*, edited by F. Schuth, K. S. W. Sing, and J. Weitkamp (Wiley-VCH, Weinheim, 2002).
[4] B. Yao and L. Zhang, J. Mater. Sci. **34**, 5983 (1999).
[5] D. R. Rolison, Science **299**, 1698 (2003).
[6] S. O. Kucheyev, T. van Buuren, T. F. Baumann, J. H. Satcher, Jr., T. M. Willey, R. W. Meulenberg, T. E. Felter, J. F. Poco, S. A. Gammon, and L. J. Terminello, Phys. Rev. B **69**, 245102 (2004).
[7] S. J. Gregg and K. S. W. Sing, *Adsorption, Surface Area, and Porosity* (Academic, London, 1982).
[8] J. J. Jia, T. A. Callcott, J. Yurkas, A. W. Ellis, F. J. Himpsel, M. G. Samant, J. Stohr, D. L. Ederer, J. A. Carlisle, E. A. Hudson, L. J. Terminello, D. K. Shuh, and R. C. C. Perera, Rev. Sci. Instrum. **66**, 1394 (1995).
[9] R. Brydson, H. Sauer, W. Engel, J. M. Thomas, E. Zeitler, N. Kosugi, and H. Kuroda, J. Phys. Condens. Matter **1**, 797 (1989).
[10] H. Zhang, M. Finnegan, and J. F. Banfield, Nano Lett. **1**, 81 (2001).
[11] F. M. F. de Groot, J. Faber, J. J. M. Michiels, M. T. Czyzyk, M. Abbate, and J. C. Fuggle, Phys. Rev. B **48**, 2074 (1993).
[12] D. W. Fischer, Phys. Rev. B **5**, 4219 (1972).
[13] L. Soriano, P. P. Ahonen, E. I. Kauppinen, J. Gomez-Garcia, C. Morant, F. J. Palomares, M. Sanchez-Agudo, P. R. Bressler, and J. M. Sanz, Monatshefte für Chemie **133**, 849 (2002).
[14] H. C. Choi, H.-J. Ahn, Y. M. Jung, M. K. Lee, H. J. Shin, S. B. Kim, and Y.-E. Sung, Appl. Spectroscopy **58**, 598 (2004).
[15] J. Guo, Int. J. Nanotechnology **1**, 193 (2004).